LBL-36621
Preprint

Lawrence Berkeley Laboratory
UNIVERSITY OF CALIFORNIA

CHEMICAL SCIENCES DIVISION

Submitted to Journal of Chemical Physics

Photodissociation of Ozone at 193nm by High-Resolution Photofragment Translational Spectroscopy

D. Stranges, X. Yang, J.D. Chesko, and A.G. Suits

December 1994

Prepared for the U.S. Department of Energy under Contract Number DE-AC03-76SF00098

DISCLAIMER

Photodissociation of ozone at 193nm by high-resolution photofragment translational spectroscopy

Domenico Stranges*, Xueming Yang, James D. Chesko and Arthur G. Suits
Department of Chemistry
University of California, Berkeley
and
Chemical Sciences Division
Lawrence Berkeley Laboratory
(December 21, 1994)

Abstract

The photodissociation of ozone has been studied at 193nm using high resolution photofragment translational spectroscopy. The results show 6 distinct peaks in the time-of-flight spectra for the O_2 product and its momentum-matched O atom counterpart. The translational energy distributions determined from the time-of-flight spectra reveal the production of a range of electronic states of the photofragments. The product electronic states were identified based on the translational energy distributions, with the aid of state-resolved imaging experiments by Houston and coworkers. The results reveal the production of a substantial yield of highly excited triplet states of O_2, recently suggested to play an important role in the stratospheric ozone balance. In addition, peaks corresponding to $O_2(a\,^1\Delta_g)$ and $O_2(b\,^1\Sigma_g^+)$ were observed, the latter confirming a previous report [A. A. Turnipseed, et al., J. Chem. Phys. **95**, 3244 (1991)]. Evidence was seen for a small contribution from the triple dissociation $O_3 \rightarrow 3O(^3P)$, and insight into the dissociation dynamics for this process was inferred from the translational energy distributions. Branching fractions and angular distributions were measured for all channels. The latter were found in general to yield negative β parameters, in contrast to what is seen at longer wavelengths.

I. INTRODUCTION

In recent years, models of stratospheric chemistry have consistently underpredicted measured ozone concentrations at altitudes from 35 to 80 km [1] and this discrepancy has come to be known as the "ozone deficit." This disagreement is surprising in view of the fact that only a handful of well-understood reactions are thought to control stratospheric ozone levels. Attempts to account for this discrepancy have recently focused on identifying new ozone sources, [2,3] since the known ozone loss mechanisms appear accurately understood and any that have been overlooked will merely increase the discrepancy. Recently a new source of stratospheric ozone has been proposed based on autocatalytic production of odd oxygen species following ozone photodissociation at wavelengths below 243 nm. [4] This suggestion was based on two observations. First, a bimodal $O(^3P)$ translational energy distribution was seen following ozone photodissociation at 226 nm, implying the coincident production of triplet O_2 containing > 4 eV internal energy; in separate experiments this excited molecular photoproduct was identified as $O_2(X\,^3\Sigma_g^-)$ in very high vibrational levels. Second, a large cross section was inferred for the reaction of vibrationally excited ground electronic state O_2 with O_2 to yield ozone, based on measurements of relaxation rates of vibrationally excited O_2. [5] The following sequence of reactions summarizes the proposed new source of ozone:

$$O_3 + h\nu_{\lambda<243nm} \rightarrow O(^3P) + O_2(X\,^3\Sigma_g^-, v \geq 26) \quad (1)$$

$$O_2(X\,^3\Sigma_g^-, v \geq 26) + O_2 \rightarrow O(^3P) + O_3 \quad (2)$$

It is significant that three odd oxygen species are produced for every ozone molecule that dissociates by this channel. Furthermore, because ozone in the stratosphere dissociates and recombines many times before any new ozone is formed or lost by established mechanisms, [6] a small quantum yield for reaction 1 may have a significant impact on the ozone budget. Although the quantum yield for reaction 1 was found to be only 0.8% at 226 nm, the process was found to produce odd oxygen at levels up to 48% that of the Chapman mechanism [7] in 2-D models. [4] We have studied O_3 photochemistry in a molecular beam at 193 nm both to confirm the bimodal distribution reported in ref. [4], and to begin a more detailed study of these "minor" channels whose atmospheric implications have been neglected.

It may seem surprising that ozone photodissociation at 193 nm has been so little studied. The reason for this is that despite the central importance of ozone in the stratosphere, the solar flux at 193 nm is low enough that dissociation there was considered unimportant. Taherian and Slanger [8] studied ozone photodissociation in a cell at 157 nm and reported a large yield of $O_2(b^1\Sigma_g^+)$ as well as a quantum yield of 0.5 for dissociation into three ground state O atoms. Ravishankara and coworkers [9] performed a detailed cell experiment at both 222 and 193 nm, and despite the fact that they measured only $O(^3P)$ or OH as a function of time and buffer gas concentration, they were able to infer a significant yield of $O_2(b^1\Sigma_g^+)$ at 193 nm, a larger yield of triplet products than seen elsewhere in the Hartley band, and some triple dissociation.

There has been considerable work done, both experimental and theoretical, in the longer wavelength regions of the Hartley band. The dominant photochemical events there are fairly

well understood as a result of several molecular beam experiments, [10,11] an extensive series of CARS experiments performed by Valentini and coworkers, [12], and resonance Raman experiments by Kinsey and others. [13,14] It is known that, in the Hartley band, the initially prepared "B" state ($^1B_2$ in C_{2v}, $\tilde{D}$ in C_s) correlates to singlet products, so these dominate (85-90%). [15] A curve-crossing is believed to be responsible for the ground electronic state products that are observed, yet these were considered atmospherically uninteresting.

There exists an extensive body of theoretical work on ozone, both *ab initio* calculations [15–22] and dynamical studies. [13–15,23–28] Owing to its electronic complexity (it is effectively a spin-paired biradical), ozone represents a serious challenge to Hartree-Fock methods. [29] Ozone's many low-lying electronic states give rise to structured and continuous absorption spectra both in the visible and the ultraviolet. Because the O_2-O bond is so weak (1.05 eV [30]) even the visible absorption may lead to photodissociation. Ozone possesses a number of novel features that have intrigued theorists over the years. The intense Hartley band represents a broad absorption peaking around 254 nm reaching a maximum of just over 10^{-17} cm^2. Dynamical calculations find a prompt impulsive dissociation generally consistent with experimental observations. [15] On top of the Hartley band continuum appears a small series of regular peaks whose origin eluded explanation for many years. Johnson and Kinsey used a harmonic analysis to study the short-time dynamics of the Hartley band dissociation, and to generate calculated absorption and Raman spectra for comparison to experiment. [14] They were able to reproduce the broad absorption, and suggest improvements to improve the shape of the "B" state surface. Imre and others performed a 2-D time-dependent calculation to generate the autocorrelation function, which they compared to results from resonance Raman experiments. [13,26,27] They found recurrences indicating that some portion of the wavefunction remains trapped in the Franck-Condon region, even though the bulk of the dissociation is over in under 100 femtoseconds. Recent 3-D time dependent calculations on a new "B" state surface have shown that this structure in the absorption spectrum is a consequence of a family of Feschbach resonances between the symmetric stretch and bending coordinate in the course of dissociation. [28] Dynamical calculations on this surface reproduce the main features of Valentini's experimental results for the singlet products, so the dominant dissociation dynamics in the center of the Hartley band are believed to be well-understood.

Ozone's complex electronic structure gives rise to a number of other novel phenomena: there exist conical intersections between the $^1A_2$ and $^1B_1$ (A'') states as well as the 1^1A_1 ($\tilde{X}$) ground state and the 2^1A_1 ($\tilde{C}$) excited state at the equilateral geometry. [18,20] A number of theoretical studies have been performed exploring the properties of a metastable D_{3h} ring from of ozone, thought to lie slightly above the dissociation threshold; [31,18] no direct experimental evidence has yet been found for this species. Virtually all dynamical studies have focused on the fate of the molecule once prepared on the $^1B_2$ surface. The details of the nonadiabatic interactions leading to ground state products have not been explored, and surface crossings leading to the various product states observed here and elsewhere represent interesting yet unexplored challenges for theorists. Some of these "minor" channels may have unanticipated consequences for atmospheric chemistry. It is our hope that these results will stimulate further theoretical studies of the nonadiabatic channels.

II. EXPERIMENTAL

These measurements were carried out on the high resolution rotating source photofragment-translational spectrometer which has been described previously in detail. [32,33] A schematic drawing of the apparatus is shown in Fig. 1. Briefly, a pulsed molecular beam of ozone seeded in helium was skimmed twice before reaching the main chamber where it was crossed at 90° by a pulsed laser beam. The neutral photofragments that flew along the detector axis were ionized by electron bombardment at a distance of 36.7 cm from the interaction region, mass selected by a quadrupole mass spectrometer, and counted with a Daly ion detector. A 486 personal computer interfaced multi-channel scaler (Turbo-MCS, EG&G Ortec), triggered from the laser pulse, was used to collect and store the Time-of-Flight (TOF) spectra. Product laboratory angular distributions were obtained by rotating the molecular beam about the laser propagation direction, which was perpendicular to the plane defined by the molecular beam direction and the detector axis.

Ozone was prepared from pure oxygen using a commercial ozonator and stored on silica gel in a glass trap at −74°C. The residual oxygen in the trap was pumped off just prior to running the experiment. A mixture of 4% ozone in helium was obtained by flowing helium over the trap warmed to −40°C. The pulsed molecular beam was generated by expanding the mixture, at a stagnation pressure of 1 atm, with a pulsed valve [34] (0.9 mm nozzle diameter) equipped with a Physik-Instrumente piezocrystal. Ozone cluster formation was drastically inhibited by adding an extension on the pulsed valve nozzle which was heated to 200 − 250°C. A water cooled copper block was used to insulate the piezocrystal from the hot tube.

The molecular beam velocity and its velocity spread were measured by time-of-flight with a spinning slotted-disk, and by the hole burning technique. By using the time-of-flight method, changing the delay between the wheel and the pulsed valve, it is possible to sample different part of the gas pulse to choose optimum experimental conditions. The delay between the pulsed valve and the laser trigger can be calculated from the wheel angular velocity and the delay between the pulsed valve and the wheel. The hole burning time-of-flight was recorded with the same setup used to detect the phofragments at different laboratory angles with background subtraction "shot-by-shot" (see below), simply by moving the source onto the detector axis with a small detector aperture (0.13 mm diameter). The beam velocity was measured to be 1350 m/s with a full-width half-maximum velocity spread of 15%.

In all the experiments the molecular beam was crossed at 90° by the output of a Lamda Physik EMG 103 MSC excimer laser operating at the ArF (193.3 nm) transition. A convex lens (25 cm focal length) was used to focus the beam to a 2.5 x 6 mm spot in the interaction region, with fluence ranging from 120-230 mJ/cm^2/pulse for studies with unpolarized light and 25-65 mJ/cm^2/pulse for studies with polarized light. The unpolarized output of the excimer laser was polarized using a pile of ten quartz plates at Brewster's angle with respect to the direction of laser propagation, yielding > 95% polarized light. The polarization direction was rotated with respect to the detector axis by adjusting the orientation of the polarizer.

Time-dependent background, arising from fragmentation of pulsed background O_3 from the molecular beam, was present in TOF's at all masses and laboratory angles. Particu-

lar care was taken in the choice of the background subtraction method used because the slowest peak in our TOF's was partially overlapping with the rising tail of the modulated background. The capacity of our multi-channel scaler to use up to 16,000 channels gave us the ability to perform background subtraction shot-by-shot. A very stable pulse generator (DG 535, Stanford Reserch Systems) was used to drive the experiment. The TTL output signal of the pulse generator was split in two coherent pulses. One was used to drive the pulsed valve, the second was frequency divided by two, delayed, and used to trigger the laser and the multi-channel scaler. Operating the pulsed valve at 50 Hz, the laser at 25 Hz, and opening a temporal window of 22 ms on the multi-channel scaler (11,000 channels, 2μs/ch) a TOF with laser on and off could be recorded at the same time. The zero time for the background TOF is defined by the repetition rate of the pulsed valve, so to get a very good background subtracted TOF it is important to use a very stable pulse generator with a jitter much less than a channel bin. In the polarization dependence experiments particularly, care has been taken to overcome systematic variations that would interfere during the long acquisition times at each polarization angle. The angular distributions were obtained by normalizing each polarization angle TOF for the laser power and integrating the area of the windows opened for each channel to minimize the overlap between two adjacent peaks. To minimize the fluctuations of the molecular beam concentration and laser power drift from scan to scan, it was decided to divide the polarization angles in different series, each of those made up of 2 or 3 polarization angles plus one reference angle common to the entire series. The polarizer was rotated every 5,000 laser shots among the angles of the series in a "pseudo random" sequence for a total of 100,000 laser shot at each angle. Each TOF in a series was normalized for the laser power and all TOF's were normalized among each other through the common reference angle. This procedure was also necessary in order to get the total angular distribution, because it was necessary to clean the lens (which is also the input window of our apparatus) between the two runs.

A forward convolution technique [33,35,36] was used to fit the data. Briefly, a trial center-of-mass translational energy distribution is convoluted with the instrumental response functions to yield a calculated TOF spectrum in the laboratory reference frame, which is then compared to the experimental one. The translational energy distribution is iteratively adjusted until a good fit is obtained.

The intensity of all detected fragments from ozone photodissociation varied linearly with laser power indicating that the observed processes involve a single photon excitation.

III. RESULTS AND ANALYSIS

Photofragment TOF spectra were collected for m/e 32 (O_2^+) at detector angles, Θ, ranging from 15° to 40° from the molecular beam, m/e 16 (O^+) at 20° and 30° and m/e 8 (O^{++}) at 20°. On all TOF's the modulated background was subtracted shot-by-shot. Given the richness of primary reaction channels present in this work, we have numbered these different contributions starting from 1 up to 6. The primary channel 1 has the highest translational energy release and will be the first one to appear on the TOF spectra while the primary channel 6 has the lowest translational energy release and will be the last one to appear on the TOF spectra (see below).

In Fig. 2, the TOF spectra collected for m/e 32 at 20°, 30°, and 40° are presented. At $\Theta = 20°$ five different peaks, centered around 100 μs, 130 μs, 160 μs, 190 μs, and 260 μs, are clearly seen. The fourth peak is actually formed from two different overlapping contributions (number 4 and 5), while the last one corresponds to the sixth channel. This can be seen at $\Theta = 30°$ where five peaks are again resolved, but here the last two correspond to channels 4 and 5, and the sixth channel is no longer visible. The Newton diagram is shown in Fig. 3, with circles representing the most probable velocities of the six different channels. The primary channel 6 has enough translational energy to be seen at $\Theta = 20°$ but not at $\Theta = 30°$, while the primary channels 4 and 5 have enough translational energy to be seen at both 20° and 30°, but at 30° their contributions are more distinct. At $\Theta = 40°$ only the first four channels are present.

The fit of the m/e 32 TOF spectrum is not enough to determine the branching ratios for the different primary channels, because the ratios among the areas of the translational energy distributions ($P(E_T)'s$) of the different contributions represent only the "apparent branching ratios", [37] that have to be corrected for the ionization cross sections and fragmentation ratios of primary O_2 photofragments. In the case of ozone photodissociation, the only counterpart masses for O_2 molecules are O atoms, so the fit to their TOF spectrum could be used to determine directly the branching ratios. However, a problem could arise from interference from the dissociatively ionized O_2 signal also appearing in the TOF spectrum at m/e 16.

In Fig. 4 the TOF spectrum of m/e 16 at $\Theta = 20°$ is shown. At this mass-to-charge ratio two different contributions are present: a faster one coming from primary O atoms and a slower one from dissociatively ionized O_2 molecules which fragment and ionize to give m/e 16. Three different regions can be identified in this spectrum: a) at shorter times only O atom signal, b) at intermediate times both O atom and fragmented O_2 molecule signals, and c) at longer times only fragmented O_2 molecule signal.

The overlapping region makes the fit of this spectrum more complex. When there are twelve different contributions, six for primary O atoms and six for O_2 fragmentation, one could easily fit the TOF spectrum simply by changing the relative ratios. However, this can yield results without physical meaning. For example, if two contributions have a given ratio at m/e 16 for the primary O atom channels and one of them fragments more at m/e 32, the ratio between these two peaks has to be higher at m/e 32 and lower at m/e 16 for O_2 fragmentation in order to be consistent, while if they have the same ratio at m/e 32 and at m/e 16 for primary O atoms, it has to be the same at m/e 16 for O_2 fragmentation (assuming that the ionization cross sections for all the O_2 channels are equal and similarly for primary O atom channels).

Our strategy to fit the m/e 16 TOF spectrum was based on this strong constraint and on a few assumptions. We have assumed that the ionization cross sections for different O_2 electronic states are the same and the ionization cross sections for the different O atom electronic states are the same (for the excited electronic states the ionization cross sections are not known). We believe that this approximation, especially for O atom electronic states, will not produce a big uncertainty in the branching ratio. In fact, the maximum atomic ionization cross sections depend on the polarizabilities, [38] which are a function of the electron cloud size. The ground $O(^3P)$ and the excited $O(^1D)$ electronic states are different spin-orbit states with the same spatial orbital; in this case the polarizability is expected to

change very little. The last assumption we made is that the fragmentation ratio of a given channel is constant in its translational energy range (or for the different degree of internal excitation of a given O_2 channel). The direct consequence of this approximation is that the shape of the $P(E_T)$ for a given primary channel used to fit the TOF spectra at m/e 32, m/e 16 primary O atoms and O_2 fragmentation is always the same.

The first two peaks in Fig. 4 centered around 60 and 75 μs correspond to the contribution of channel 1 and 2 for primary O atoms and they do not overlap with any O_2 fragmentation signal. A good fit of these two peaks at m/e 16 is obtained using the same ratio between the $P(E_T)$'s used for m/e 32 (Fig. 2). This result automatically fixes the ratio for the same O_2 fragmentation peaks. The next step is to fit the two features centered around 100 and 125 μs. In this region there are the overlapping contributions of channel 3 and 4 from primary O atoms and channel 1 and 2 from O_2 fragmentation. In an attempt to obtain a "clean" primary O atom TOF spectrum, we recorded the spectrum of m/e 8 (O^{++}) at the same angle (Fig. 5), since primary O atoms are much more likely to appear as doubly charged ions than are fragments of O_2. Unfortunately, the O_2 fragmentation contribution is still present, even if it is strongly decreased. However this spectrum is very useful because we can define an upper limit for the ratios: channel 3/channel 2 and channel 4/channel 2 of primary O atoms. Using these two new constraints and the fixed ratio between channel 1 and channel 2 for O_2 fragmentation, a good fit is obtained. Again we found that the ratio between channel 3 and channel 2 for primary O atoms is the same as that used for m/e 32, while the ratio channel 4/channel 2 for primary O atoms is higher than that used for m/e 32. Two conclusions follow: the ratio channel 3/channel 2 for O_2 fragmentation must be the same as what is found for primary O atoms and for m/e 32, while the ratio channel 4/channel 2 for O_2 fragmentation must be bigger than what is found for primary O atoms and even bigger for the m/e 32 peaks. Following this strategy, the rest of the TOF spectrum was fitted and the total calculated TOF is shown as a heavy dashed line in Fig. 4. As can be seen in this figure there are two regions of the TOF (around 150 and 220 μs) where the fit is poor because the calculated contribution is less than the experimental one. The only way to improve the fit around 150 μs is to increase the weighting of channel 3 for O_2 fragmentation. However, this is not physically reasonable based on what we found before in fitting primary O atoms and m/e 32. In the region around 220 μs there is no way to improve the fit because there are no channels that contribute appreciably in this region. The only possibility for the presence of extra signal at m/e 16 is the dissociation of O_3 forming three ground state O atoms:

$$O_3 + h\nu \rightarrow 3\,O(^3P) \tag{3}$$

The available energy for the triple dissociation can be calculated from the dissociation energy of O_3 and O_2:

$$E_{avail} = E_{h\nu} - D_0(O_2{-}O) - D_0(O{-}O) \tag{4}$$

If one takes the bond dissociation energy of ozone (O_2–O) [30] to be 24.2 kcal/mol and uses standard values for the bond energy of O_2, [39] the thermodynamic threshold for the triple dissociation is 142.2 kcal/mol. The photon energy for λ=193.3 nm is 147.9 kcal/mol,

so 5.7 kcal/mol is the available energy for the three O atoms recoiling in the center-of- mass reference frame.

The triple dissociation could follow two different limiting mechanisms. It could be a sequential two body dissociation (secondary dissociation) or a concerted dissociation of both bonds. The difference between these two mechanisms is the time interval between the rupture of the two bonds. If the O_2 molecule formed after the breaking of the first bond lives long enough, often taken to be a time on the order of a rotational period or longer, the triple dissociation can be considered a two step mechanism. If, however, the lifetime of the O_2 molecule is much shorter than its rotational period it can be considered a concerted mechanism. [40] In the case of ozone it is quite apparent that the triple dissociation has to be concerted, because the "nascent hot O_2" will have enough internal energy to break apart, and this will happen in one vibrational period or less, much shorter than a rotational period.

A method for the analysis of a synchronous three-body dissociation was recently developed for the study of s-tetrazine. [35,41] Briefly, the experimental data is analyzed by the same forward convolution technique used to fit two- body dissociations but with several important differences. An energy independent set of most probable angles among the asymptotic velocity vectors is chosen, with gaussian functions describing the spread about these angles. For a perfectly monochromatic laser beam a delta function for the $P(E_T)$ should be used, but we have used a gaussian $P(E_T)$ centered at 5.7 kcal/mol to reproduce the bandwidth of our excimer laser emission. The only parameters that can be changed in the simulation are the angles among the asymptotic velocity vectors. The triple dissociation contribution improves the fit of the TOF (Fig. 4) in both regions at the same time. In Fig. 6, a schematic velocity space diagram for the triple dissociation is shown, indicating the combination of recoil velocities that gave the best fit to the experimental data.

The fits of m/e 32 and m/e 16 TOF's, following the above strategy, show that the fragmentation ratios of all the two-body dissociation channels except one are the same; for channel 4 it is twice as large as all the others (see Discussion section).

The branching ratio between two given channels depends also on the anisotropy parameter, even if unpolarized light is used. [42] In Fig. 7 the laboratory angular distributions for the different channels are presented. The polarization direction of the light is rotated in the plane defined by the molecular beam and the detector axis. The laboratory polarization angle (γ), the angle between the electric vector $\mathbf{E}$ and the photofragment laboratory velocity vector $\mathbf{v}$ (detector axis), was varied every 20°, from 0° to 180°. Polarization dependence studies were done for m/e 32 at two different laboratory angles, $\Theta = 20°$ and $\Theta = 30°$, because at 20° channel 4 and 5 overlap, while at 30° they do not but channel 6 is no longer present. The laboratory angular distributions for the different channels are obtained from the normalized TOF's recorded at different polarization angles by opening a temporal window and integrating the signal for each channel in order to minimize the overlapping contributions. The anisotropy parameter, β is obtained directly from the laboratory angular distribution [43,44] $I(\gamma)$:

$$I(\gamma) = A[1 + \beta P_2(\gamma - \gamma_0)] \tag{5}$$

where γ_0 is the correction angle for the center-of-mass to laboratory transformation, $P_2(\gamma - \gamma_0)$ is the second Legendre polynomial in $\cos(\gamma - \gamma_0)$ and A is a normalization factor.

The three parameters A, β, and γ_0 were obtained by a least-squares fit to the experimental data, and the results for the different channels are presented in Table I. An indication of the quality of the fit of the angular distributions can be obtained by estimating the correction angle γ_0 from the molecular beam velocity, the laboratory photofragment velocity and the angle Θ. The agreement is very good.

In Fig. 8 the $P(E_T)$'s for the single primary photofragment channels used to fit the TOF spectra at different angles and mass-to-charge ratios are reported. From the area underlying each $P(E_T)$ the branching fraction for each channel is obtained, and shown in Table I. The triple dissociation channel branching fraction has been obtained by running the three- body dissociation analysis program (CMLAB1) [35,41] with a "reference" two-body dissociation channel and using the same anisotropy parameter as channel 4 (see Discussion section). All the numeric information of the $P(E_T)$'s are also presented in Table I.

IV. DISCUSSION

A. Branching fractions and assignments

The $P(E_T)$ distribution (figure 8) obtained by fitting the TOF spectra in figures 2 and 4 were used as described to obtain branching fractions into the various product channels. These are summarized in Table I, along with assignments of the corresponding channels. The assignment of each channel will be considered in turn, beginning with the fastest (highest E_T) first.

1. Channel 1

The fastest channel clearly corresponds to the production of ground electronic state O_2 and $O(^3P)$. This identification is based on a number of observations: 1) the $P(E_T)$ obtained from both imaging [4] and Doppler [45] measurements of the $O(^3P)$ fragment from 226 nm dissociation of ozone showed a similar broad, high energy component, shifted by the 15.0 kcal difference in available energy; 2) imaging results for the $O(^3P)$ fragment at 193 nm [46] showed two peaks, one of which matched this one; and 3) the fastest peak obviously corresponds most likely to the production of ground electronic state products.

The molecular product is probably in a broad range of excited vibrational levels, consistent with results reported elsewhere in the Hartley band. [4,47,45] If we assume a rotationally impulsive dissociation, the fraction of available energy appearing in rotation is variously given in the range of 15 to 23%. [12,47] For the maximum of the peak, the translational energy release corresponds to 68 kcal/mol. If this represents 77 to 85% of the avalable energy (not including vibration) then the energy in rotation is in the range 12 to 20 kcal/mol, corresponding to $J = 53 - 69$ Taking the intermediate value can thus infer the most probable vibrational level to be roughly v=19, with a very broad range of levels populated. This substantial vibrational excitation is not surprising since these products originate in a nonadiabatic transition from the initial $\tilde{D}$ surface (C_s) to the $\tilde{C}$ surface correlating to ground state products. The vibrational state distribution is thus determined by Franck-Condon factors at the crossing seam. The branching fraction obtained is 16% for this channel, slightly higher

than reported elsewhere in the Hartley band, [11,12] but consistent with a nonadiabatic transition coupled with a higher velocity through the crossing region.

2. Channel 2

The second channel is the dominant one, accounting for nearly half of all product flux. This channel is clearly associated with the production of $O(^1D)$ and $O_2(a\,^1\Delta_g)$, the products that adiabatically correlate to the upper $\tilde{D}$ surface. This assignment is based on several observations: 1) the translational energy release, discussed below, is in accord with what is expected for this channel; 2) no analogous channel was seen in the photofragment imaging of $O(^3P)$ at 193 nm, suggesting that it is indeed a singlet peak and 3) an analogous peak was seen in a photofragment imaging experiment at 205 nm, in which the translational energy release for $O(^1D)$ was measured. [46]

The translational energy release at the peak is 35 kcal/mol, leaving 21 kcal/mol for internal energy of the $O_2(a\,^1\Delta_g)$. From previous work it is believed that in the Hartley band this channel is largely vibrationally adiabatic, peaking strongly at $v = 0$. This is because the preserved O-O bond length is little changed on going from the O_3 equilibrium configuration (1.271 Å) to the product $O_2(a\,^1\Delta_g)$ (1.215 Å). [12] If in this case, too, the $O_2(a\,^1\Delta_g)$ product is predominantly in the ground vibrational level, then the rotational energy peaks at 21 kcal/mol, corresponding to $J = 70$. This (37%) is a larger fraction of energy in rotation than is seen at the longer wavelengths, and significantly larger than is expected based on a simple rotationally impulsive model (23%). Alternatively, if we assume the rotational distribution peaks at the value given by the impulsive model ($J = 54$), the vibrational distribution must peak at v=1 rather than v=0. This is not implausible, even for dissociation on the same $\tilde{D}$ surface, since we now have more than 56 kcal/mol available energy (more than twice that at the highest energy studied in Valentini's experiments). The "vibrationally adiabatic" picture may break down if a sufficient portion of the initial impulse is directed along the preserved bond to produce vibrational excitation.

Although Turnipseed et al. inferred from their experiments that there was no contribution from this channel at 193 nm, this conclusion was simply based on the fact that their observed $O_2(b\,^1\Sigma_g^+)$ and $O(^1D)$ quantum yields were quite similar. Our observations are not inconsistent with their results since our $O_2(b\,^1\Sigma_g^+)$ yield lies in the lower range of their quoted error, while our $O(^1D)$ yield is in the upper range of their error bounds. The difference between these two is sufficient to account for a sizable yield of $O_2(a\,^1\Delta_g)$.

3. Channel 3

The third peak was not observed in the imaging of the triplets at 193 nm, nor in the singlets at 205 nm, [46] strongly suggesting that it is a singlet channel with onset between 205 and 193 nm. It is assigned as $O(^1D) + O_2(b\,^1\Sigma_g^+)$, in accord with the observed translational energy release and the findings of Turnipseed et al. [9] However, while we find a branching fraction of 23.3%, the latter reported a quantum yield of 0.50 ± 0.38 for this channel. The translational energy release is shifted 13.8 kcal/mol from that of the channel assigned as $O(^1D) + O_2(a\,^1\Delta_g)$, precisely equal to the electronic energy splitting between $O_2(a\,^1\Delta_g)$

and $O_2(b\,^1\Sigma_g^+)$. This suggests a similar product state distribution for both channels. As discussed above, this most likely implies a rotationally impulsive dissociation peaking at $v = 1$.

4. Channel 4

The fourth channel is assigned as highly vibrationally excited $O_2(X\,^3\Sigma_g^-)$ based on the following observations: A slow component in the recoil velocity distribution was previously reported for the triplet channel at 226 nm and found, based on direct probing of the nascent products in a cell experiment, to correspond to the production of highly vibrationally excited, ground electronic state O_2. [4,45] In addition, the $P(E_T)$ for this channel cuts off precisely at the threshold for triple dissociation, implying that it involves the formation of a ground state oxygen atom. Finally, a strong peak at the same energy was observed in the imaging of $O(^3P)$ at 193 nm, confirming it as a triplet channel. [46]

This peak appears in the vicinity of the threshold for the production of $O(^3P)$ + $O_2(A\,^3\Sigma_u^-)$, so some remarks on its assignment as ground electronic state O_2 are warranted. The bimodal translational energy distribution observed in the 226 nm experiments was seen also at longer wavelengths, [4] below the threshold for the formation of the ungerade states of O_2. This represents some of the strongest evidence that it is indeed ground electronic state O_2, since it is conceivable that quenching of these excited states could be fast enough that the cell experiments might detect only ground state O_2. Further evidence is found in the TOF spectra for m/e 32, 16 and 8 shown in Figs. 3-5, and the corresponding analysis of the fragmentation patterns for the different channels. As mentioned in the Results and Analysis section, the m/e 16 TOF contains contributions from the oxygen atom and from fragmentation of the oxygen molecules in the ionizer. Good fits to the TOF spectra for m/e 32 and momentum-matched m/e 16 were obtained by assuming that the fragmentation ratios for all O_2 channels were essentially the same, except for the fourth channel. The latter was found to be twice as likely to fragment to give m/e 16 as the others. Although the fragmentation patterns for 200 eV electron bombardment of $O_2(X\,^3\Sigma_g^-, v > 25)$ and $O_2(X\,^3\Sigma_u^-)$ are both unknown, we suggest that this enhanced fragmentation indicates that the product is vibrationally rather than electronically excited. The additional 4 eV in nuclear motion effectively promotes fragmentation on electron bombardment. The yield of this channel at 193 nm was found to be 7.3% nearly a factor of 10 higher than found at 226 nm. A significant contribution from an additional triplet channel is also in accord with the previous report of a total yield of triplets of 50%. [9]

5. Channels 5 and 6

Channels 5 and 6 will be considered together, since they appear to be related and their precise identity is somewhat speculative. They are both very narrow peaks that occur above the threshold for triple dissociation. This implies that they cannot involve the formation of ground electronic state O atom. The next likely candidate then is formation of $O(^1D)$. The corresponding partners for spin allowed channels are the same as those responsible for channels 2 and 3, viz., $O_2(a\,^1\Delta_g)$ or $O_2(b\,^1\Sigma_g^+)$. Although these are possibilities, the former

seems particularly unlikely since the peaks are so narrow (only slightly broader than the linewidth determined by the photolysis laser), while the energy available to this channel is greater than 34 kcal/mol. The first plausible candidate is vibrationally excited $O_2(b\,^1\Sigma_g^+)$. Vibrational levels on the order of 4 or 5 would be consistent with the translational energy release, depending on the rotational excitation. Again, however, the narrowness of these peaks implies a very narrow range of excited rotational levels, and this is difficult to explain. A final possibility is the formation of the next higher singlet O atom, $O(^1S)$ in conjunction with $O_2(a\,^1\Delta_g)$. Channel 5 occurs just at the threshold for this channel, as indicated in figure 8. In addition the spacing between the peaks, 3.25 kcal/mol, is close to the v 0,1 vibrational spacing $O_2(a\,^1\Delta_g)$ (4.3 kcal/mol). If this assignment is correct, however, the products must be rotationally cold and this is difficult to justify. One possible mechanism for the formation of rotationally cold products is the departure of the central oxygen atom. Although this could simultaneously account for the appearance of a different electronic channel, it is difficult to reconcile the angular distributions, discussed below, with such a mechanism for this channel. The final difficulty with assignment of these as $O(^1S)$ is a study by Taherian and Slanger. [8] This work placed an upper limit of .1% on $O(^1S)$ yield from ozone photolysis in the range from 120 to 240 nm. We observe a branching fraction of $> 4\%$ for the total of these two channels. This cannot readily be reconciled with the work of Taherian and Slanger even at the limits of the quoted error. Clearly some further investigation is required for unambiguous assignment of these peaks.

6. Triple dissociation

As indicated in the Results and Analysis section, fits of the m/e 16 TOF spectra were unsatisfactory when strict momentum-matching of the m/e 32 results and plausible fragmentation patterns were enforced. A small yield (2.0%) for a "concerted" triple dissociation process was found to give contributions precisely in the regions where the fits were inadequate. This is again consistent with the results of Ravishankara's group at 193 nm and Taherian and Slanger at 157 nm. The former reported a quantum yield for O atoms of $1.20 \pm .15$ while at 157 nm the triple dissociation yield jumps to 50%.

B. Angular distributions

The angular distributions for each channel are shown in figure 7, and the corresponding β values are compiled in Table I. The results show that for all but the fastest peak, the dissociation is closer to perpendicular rather than parallel, with the β's clustered in the range of -0.29 to -0.40. This is surprising in view of the fact that the $\tilde{D}$, $\tilde{C}$ and $\tilde{R}$ states, the only likely candidates for electronic transitions in this region, possess transition moments predominantly oriented perpendicular to the C_{2v} axis and in the molecular plane (M_y type transition). Prompt dissociation from the ground state equilibrium geometry would yield $\beta = 1.18$ for dissociation in the Hartley band. [44] Previous measurements in the Hartley band reveal positive β values that are substantially lower than this, ranging from $\beta = 0.7$ (reported at 226 nm) [45] to 1.0 (for the singlet channel at 274 nm). [10] For M_y type transitions in the limit of prompt recoil these correspond to bond angles of 98° and 109°,

respectively. This is not likely to be attributable to rotational erosion since the dissociation is over in 50 femtoseconds, long before any rotational effects would show up in the β parameter. A more likely explanation is that a significant change in bond angle occurs on electronic excitation. Recent fully three-dimensional time-dependent dynamics calculations on a high quality *ab initio* surface provide insight into these trends. [28] The Franck-Condon region of the newer "B" state surface is much steeper in the bending coordinate than previous surfaces. The dynamical consequence of this is that the wavepacket "rushes out of the region of the equilibrium bond angle" within the first 10 fs following electronic excitation. The theoretical calculations found bond angles in the range $86 - 96°$ for dissociation in the Hartley band, although the photolysis energy was not explicitly given.

Although the calculations make clear why the β's in the Hartley band have been found to be lower than expected based on impulsive dissociation from the ground state geometry, it may still be difficult to account for the *negative* β values we observe at 193 nm. The range of β's seen for channels 2-6, correspond to a bond angles around 58° for an M_y type electronic transition. Although this is quite close to the equilateral configuration, and there is a conical intersection in the vicinity of this geometry, it is unlikely that this has any direct bearing on the observed angular distributions. One might be tempted to look for other electronic transitions that might more readily give negative β's. However, even allowing for other orientations of the transition moment one would be challenged to find a plausible alternative scenario giving $\beta = -0.4$. A final suggestion might be the departure of the central O atom. Although this is certainly conceivable, we see no direct evidence of this. The angular distributions, again in the prompt limit, would then be either pure perpendicular (for an M_x or M_y transition), or pure parallel (for an M_z transition). We believe the most likely explanation for the observed angular distributions is the same as that seen elsewhere in the Hartley band: an upper state that is very steep in the bending coordinate resulting in rapid shrinking of the bond angle prior to dissociation.

C. Dissociation dynamics

We now consider the implications of these results for ozone dissociation dynamics at 193 nm. The first question of interest concerns the nature of the electronic state or states responsible for the absorption. This wavelength falls in the vicinity of a local minimum in the ozone absorption spectrum, between the Hartley band and an intense VUV absorption. Recent *ab initio* calculations on the full range of electronic states in this energy regime [20,21] show that, although the Hartley band maximum clearly corresponds to vertical transitions to the $\tilde{D}$ state from the equilibrium geometry, in the vicinity of 193 nm significant contributions could arise from the $\tilde{C}$ and $\tilde{R}$ surfaces. The fact that the singlet channel correlating the $\tilde{D}$ surface continues to dominate here suggests that here transitions to the $\tilde{D}$ surface continue to prevail. In addition, the fast triplet channel (channel 1) probably has the same origin as the triplet component seen in the Hartley band, viz., a nonadiabatic transition from the $\tilde{D}$ surface to the $\tilde{C}$ surface in the course of the dissociation. Channel 1 thus corresponds to transitions to the $\tilde{D}$ state as well.

The upper state responsible for the third channel, assigned to $O(^1D) + O_2(b^1\Sigma_g^+)$, is less clear. There have been no calculations on surfaces higher than the $\tilde{R}$ state, and none that

reveal correlations to this channel. The fact that we find a yield of 23% at 193 nm, and this apparently grows to 50% at 157 nm, suggests that there is a distinct transition to another electronic state, and it may be responsible for some of the strong VUV absorption. In fact, the transition could be to the $\tilde{R}$ state which is then somehow strongly coupled to another surface correlating to these products.

Based on the increase we observe in the channel giving very hot ground state products on going from 226 to 193 nm, we can make some inferences regarding its origin. The calculations of Banichevich et al. show that at this energy transitions to the $\tilde{C}$ and the $\tilde{R}$ state may occur from asymmetrically distorted geometries, and the calculated transition moments are of a magnitude comparable to those to the $\tilde{D}$ surface. [21] The $\tilde{C}$ surface correlates to ground state products, so this represent a clear mechanism for the formation of these products with an internal energy distribution distinct from that of channel 1. Alternately, theoretical calculations find a conical intersection between the $\tilde{C}$ state and the ground state, in the vicinity of the equilateral geometry. [18,20] This represents another distinct path to ground state products from the $\tilde{C}$ surface. However, the calculations have not been sufficiently extensive to allow meaningful speculation about the fact that so much of the available energy for this channel appears in vibration. No surfaces correlating to $O(^1S)$ have been calculated, either, so speculation on transitions leading to such products is unwarranted. The triple dissociation channel appears likely to have the same origin as the channel giving hot ground state O_2, since it represents simply a continuation of this channel into the O_2 dissociative continuum. It is likely that this is the $\tilde{C}$ surface, following the arguments given above.

The fit to the triple dissociation channel yields some information on the dissociation dynamics as well. Because it represents concerted dissociation of a triatomic, it must be a nearly synchronous process: that is, the second O-O bond must break within a single vibrational period following breaking of the first. From the fits it is clear that there are two distinct O atom velocity distributions for this channel, one fast and one slow. The best fits were obtained with the recoil velocities shown in figure 6. This configuration implies a prompt repulsive interaction predominantly between two O atoms, with the third acting nearly as a spectator: little momentum is exchanged between the first two and the third. One should be cautioned from inferring anything directly about the transition state geometry from these recoil vectors, however, since they may incorporate the influence of exit channel forces, and will be sensitive to the timing of the two bond ruptures.

The angular distributions are somwhat puzzling, however, if we ascribe the different observed channels to distinct upper electronic states. All of the observed β values are remarkably similar except that of channel 1. The more isotropic distribution seen for channel 1 may be easily rationalized as a consequence of a nonadiabatic interaction that is favored for larger bond angles. The fact that the other β's are so similar implies either that they all share the same transition (which we have argued against) or that the upper states are sufficiently similar, at least in the bending coordinate, to yield similar angular distributions. Unfortunately, to date there have not been sufficiently detailed calculations for bond angles outside of the equilibrium geometry to yield much insight on this question.

V. CONCLUSIONS

Results have been presented for ozone photodissociation at 193 nm showing production of a range of product electronic states. The product states were identified based on their translational energy distributions and state-resolved imaging experiments by Houston and co-workers. Among the product channels observed was one corresponding to the production of a substantial yield of highly excited triplet states of O_2, recently suggested to play an important role in the stratospheric ozone balance. In addition, channels corresponding to $O_2(a\,^1\Delta_g)$ and $O_2(b\,^1\Sigma_g^+)$ were observed as well as a contribution possibly representing the channel $O(^1S)+O_2(a\,^1\Delta_g)$. Evidence was seen for a small contribution from the triple dissociation $O_3 \rightarrow 3O(^3P)$ previously reported by Ravishankara and coworkers, and insight into the dissociation dynamics for this process inferred from the translational energy distributions. Branching fractions and angular distributions were presented for all channels. The dissociation dynamics, including the upper states responsible for the transitions, were discussed in light of recent theoretical calculations.

ACKNOWLEDGMENTS

D.S. gratefully acknowledges the *Consiglio Nazionale delle Richerche* (Italy) for a fellowship. AGS thanks Simon North for comments on the manuscript. This work was supported by the Director, Office of Energy Research, Office of Basic Energy Sciences, Chemical Sciences Division of the U. S. Department of Energy under contract No. DE-ACO3-76SF00098.

REFERENCES

* Permanent address: Dipartimento di Chimica, Universitá "La Sapienza", Rome.

[1] J. Eluszkiewicz and M. Allen, J. Geophys. Res. **98**, 1069 (1993).

[2] J. E. Frederick and R. J. Cicerone, J. Geophys. Res. **90**, 10733 (1985).

[3] T. G. Slanger, L. E. Jusinski, G. Black, and G. E. Gadd, Science **241**, 945 (1988).

[4] R. L. Miller *et al.*, Science **265**, 1831 (1994).

[5] J. M. Price, J. A. Mack, C. A. Rogaski, and A. M. Wodtke, Chem. Phys. **175**, 83 (1993).

[6] P. Warneck, *Chemistry of the Natural Atmosphere* (Academic Press, London, 1988).

[7] S. Chapman, Q. J. R. Meteorol. Soc. **3**, 103 (1930).

[8] M. R. Taherian and T. G. Slanger, J. Chem. Phys. **83**, 6246 (1985).

[9] A. A. Turnipseed *et al.*, J. Chem. Phys. **95**, 3244 (1991).

[10] C. E. Fairchild, E. J. Stone, and G. M. Lawrence, J. Chem. Phys. **69**, 3632 (1978).

[11] R. K. Sparks *et al.*, J. Chem. Phys. **72**, 1401 (1980).

[12] J. J. Valentini *et al.*, J. Chem. Phys. **86**, 6745 (1987).

[13] D. Chasman, D. J. Tannor, and D. G. Imre, J. Chem. Phys. **89**, 6667 (1988).

[14] B. R. Johnson and J. L. Kinsey, J. Chem. Phys. **87**, 1525 (1987).

[15] P. J. Hay, T. R. Pack, R. B. Walker, and E. J. Heller, Amer. Chem. Soc. (1982).

[16] P. J. Hay and J. T. H. Dunning, J. Chem. Phys. **67**, 2290 (1977).

[17] M. G. Sheppard and R. B. Walker, J. Chem. Phys. **78**, 7191 (1983).

[18] S. S. Xantheas, G. J. Atchity, S. T. Elbert, and K. Ruedenberg, J. Chem. Phys. **94**, 8054 (1991).

[19] A. Banichevich, S. D. Peyerimhoff, and F. Grein, Chem. Phys. Lett. **173**, 1 (1990).

[20] A. Banichevich and S. D. Peyerimhoff, Chem. Phys. **174**, 93 (1993).

[21] A. Banichevich, S. D. Peyerimhoff, and F. Grein, Chem. Phys. **178**, 155 (1993).

[22] K. Yamashita, K. Morokuma, F. L. Quéré, and C. Leforestier, Chem. Phys. Lett. **191**, 515 (1992).

[23] D. J. Tannor, J. Am. Chem. Soc. **111**, 2772 (1989).

[24] F. LeQuéré and C. Leforestier, J. Chem. Phys. **92**, 247 (1990).

[25] S. C. Farantos and H. S. Taylor, J. Chem. Phys. **94**, 4887 (1991).

[26] B. R. Johnson and J. L. Kinsey, Phys. Rev. Lett. **62**, 1607 (1989).

[27] B. R. Johnson and J. L. Kinsey, J. Chem. Phys. **91**, 7638 (1989).

[28] C. Leforestier *et al.*, J. Chem. Phys. **101**, 3806 (1994).

[29] P. J. Hay, T. H. D. Jr., and W. A. G. III, J. Chem. Phys. **62**, 3912 (1975).

[30] P. Gunther, W. Wassmuth, and L. A. Schyver, Z. Phys. Chem. **158**, 297 (1932).

[31] S. S. Xantheas, S. T. Elbert, and K. Ruedenberg, J. Chem. Phys. **93**, 7519 (1990).

[32] A. M. Wodtke and Y. T. Lee, J. Chem. Phys. **89**, 4744 (1985).

[33] A. M. Wodtke (unpublished).

[34] D. Proch and T. Trickl, Rev. Sci. Instrum. **60**, 713 (1989).

[35] X. Zhao (unpublished).

[36] X. Zhao, G. M. Nathanson, and Y. T. Lee, Acta Physico-Chimica Sinica **8**, (1992).

[37] A. M. Schmoltner (unpublished).

[38] R. E. Center and A. Mandl, J. Chem. Phys. **57**, 4104 (1972).

[39] K. P. Huber and G. Herzberg, *Molecular Spectra and Molecular Structure Constants of Diatomic Molecules* (Van Nostrand Reinhold Company, Inc., ADDRESS, 1979).

[40] C. E. M. Strauss and P. L. Houston, J. Phys. Chem. **94**, 8751 (1990).
[41] X. Zhao, W. B. Miller, E. J. Hintsa, and Y. T. Lee, J. Chem. Phys. **90**, 5527 (1989).
[42] J. G. Frey and P. Felder, Molec. Phys. **75**, 1419 (1992).
[43] G. E. Busch and K. R. Wilson, J. Chem. Phys. **56**, 3638 (1972).
[44] R. N. Zare, Molec. Photochem. **4**, 1 (1972).
[45] T. Kinugawa *et al.*, J. Chem. Phys. **93**, 3289 (1990).
[46] A. G. Suits, R. L. Miller, S. Rogers, and P. L. Houston (unpublished).
[47] M. J. Daniels and J. R. Wiesenfeld, J. Chem. Phys. **98**, 321 (1993).

TABLES

TABLE I. Summary of results from fitting TOF and angular distributions. R is the branching fraction, f_{E_T} is the fraction of the available energy appearing in translation, E_T is the most probable translational energy, and E_{avail} is the total energy available. Energies in kcal/mol. Quoted error in the β parameters are one standard deviation in the least squares fit, and that in the branching fraction is based on the sensitivity of the fit.

Channel	Assignment	β	$R(\%)$	$< E_T >$	$f_{E_T}(\%)$	E_T (Peak)	E_{avail}
1	$O_2(X\,^3\Sigma_g^-) + O(^3P)$	$.09 \pm .03$	16.8 ± 1.5	71.0	57.4	59.0	123.7
2	$O_2(a\,^1\Delta_g) + O(^1D)$	$-.32 \pm .01$	45.5 ± 2.5	35.0	62.7	34.0	55.8
3	$O_2(b\,^1\Sigma_g^+) + O(^1D)$	$-.29 \pm .03$	23.3 ± 2.0	18.0	44.1	18.5	40.8
4	$O_2(X\,^3\Sigma_g^-, hot) + O(^3P)$	$-.33 \pm .02$	7.7 ± 0.6	8.3	6.7	8.50	123.7
5	$O_2(a\,^1\Delta_g, v=0) + O(^1S)$	$-.38 \pm .04$	2.1 ± 0.5	5.8	> 100	6.00	4.6
6	$O_2(a\,^1\Delta_g, v=1) + O(^1S)$	$-.40 \pm .09$	2.6 ± 0.5	2.8	61.4	2.75	0.4
Triple	$3\ O(^3P)$	$-.33 \pm .02$	2.0 ± 0.2	5.7	100	5.7	5.7

FIGURES

FIG. 1. Schematic view of apparatus. Photolysis laser is directed perpendicular to the plane of the figure. PV, pulsed valve; DET, detector; $\vec{E}$, direction of the electric vector of the laser. The polarization angle γ, is defined with respect to the detector axis as shown, and the laboratory scattering angle, Θ, is the angle between the molecular beam and the detector axis.

FIG. 2. Time-of-flight of m/e 32, O_2^+, from photodissociation of ozone at 193 nm at the indicated laboratory angles. The circles are experimental points, the dotted lines are the contributions from each channel in the simulation, and the solid line is the sum of all 6 contributions in the simulation.

FIG. 3. Newton diagram for ozone photodissociation at 193 nm. The six circles represent the observed most probable recoil velocities for the m/e 32 product for the six channels described in the text.

FIG. 4. Time-of-flight of m/e 16, O^+, from photodissociation of ozone at 193 nm at $\Theta = 20°$. The light solid lines represent the calculated contribution from primary O atoms for the indicated channel. The dotted lines give the contributions from fragmentation of O_2 for the indicated channel. The dot-dash line shows the contribution from triple dissociation. The heavy dash line is the total fit without the contribution from triple dissociation, and the heavy solid line is the total simulation including triple dissociation.

FIG. 5. Time-of-flight of m/e 8, O^{++}, from photodissociation of ozone at 193 nm at $\Theta = 20°$, showing the simulated contributions from the first four primary O atom channels.

FIG. 6. Combination of recoil velocity vectors used to fit the triple dissociation $O_3 + h\nu \rightarrow 3O(^3P)$, along with corresponding energy release parameters.

FIG. 7. Angular distributions for the 6 channels, numbered according to the text. Points are experimental values, solid lines are the fit as described, with resulting β values shown for each data channel.

FIG. 8. $P(E_T)$ distribution (total center-of-mass translational energy release) for $O_3 + h\nu_{193nm} \rightarrow O_2 + O$ obtained from the data in Figs. 3-5. Thresholds are shown for the spin-allowed dissociation channels.

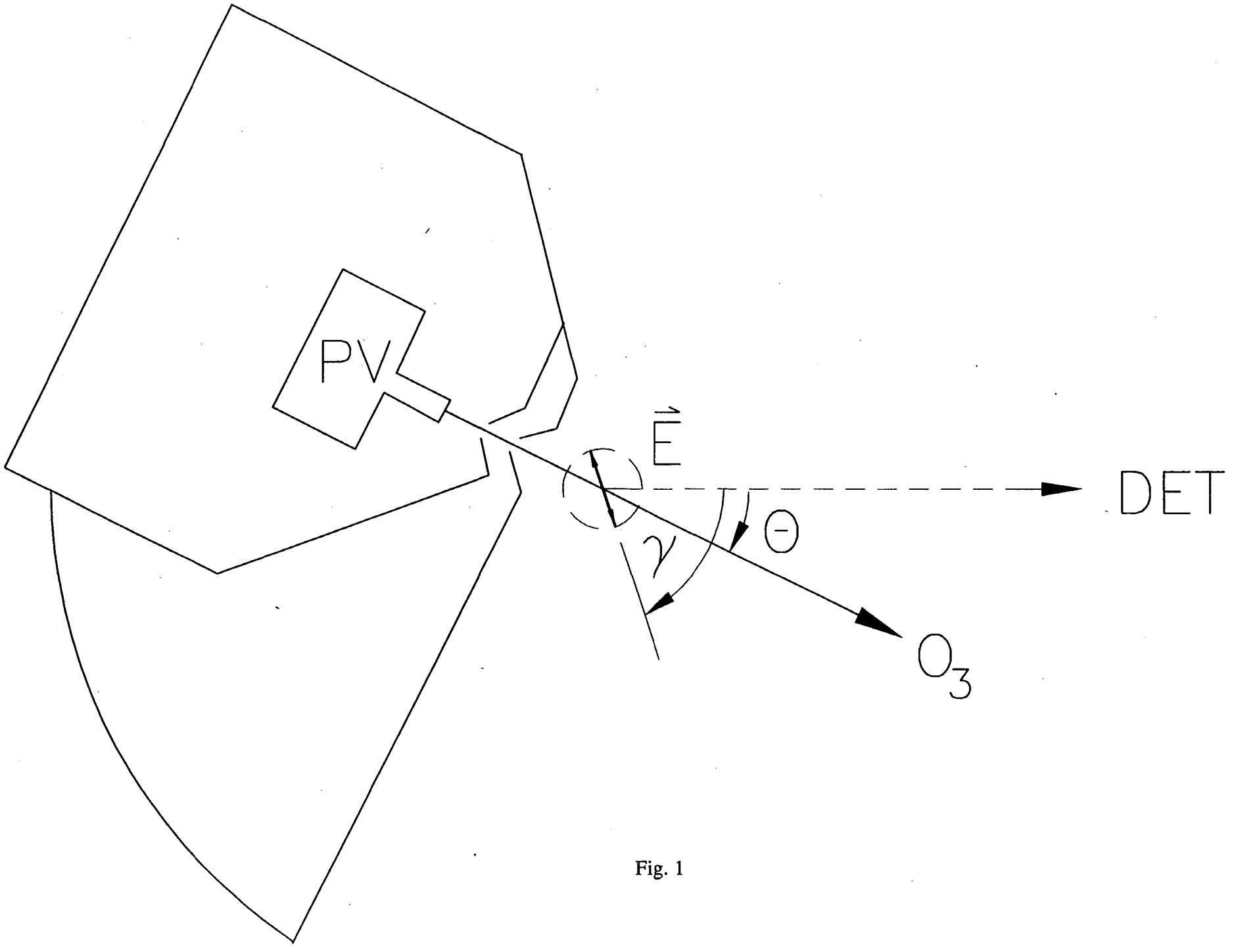

Fig. 1

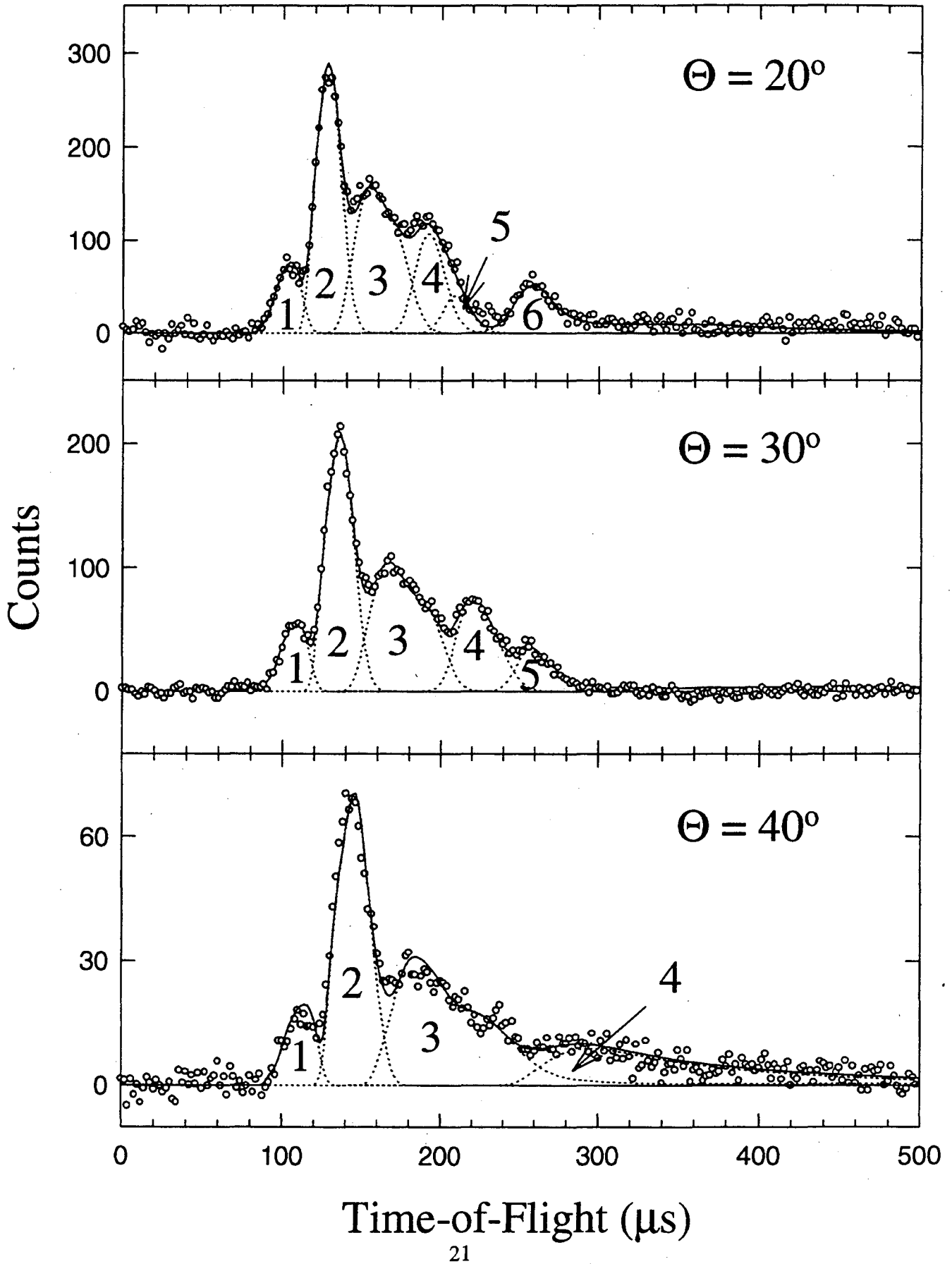
Θ = 20°
Θ = 30°
Θ = 40°
Counts
Time-of-Flight (μs)
1
2
3
4
5
6
0
100
200
300
400
500
60
30

Fig. 2

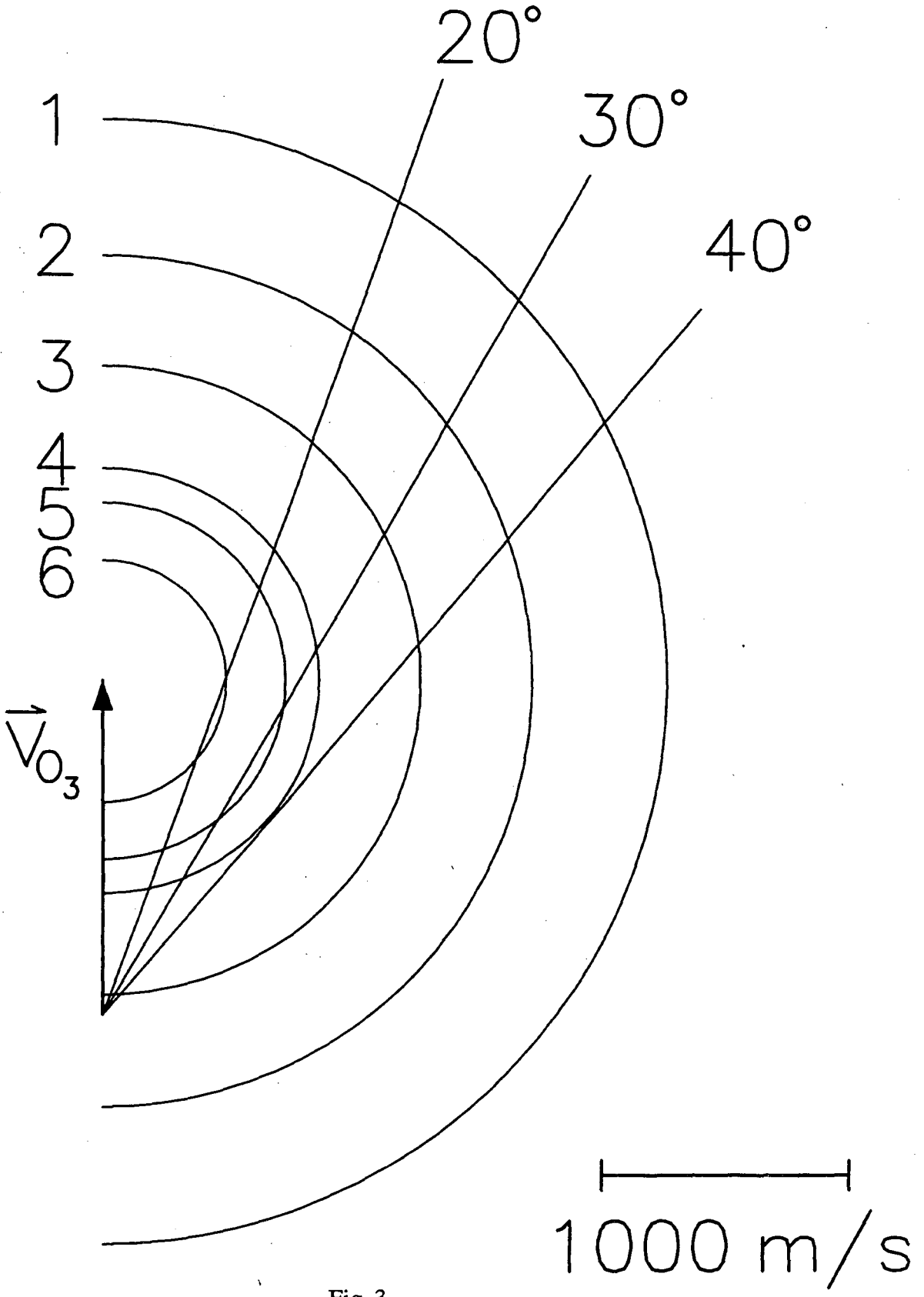

Fig. 3

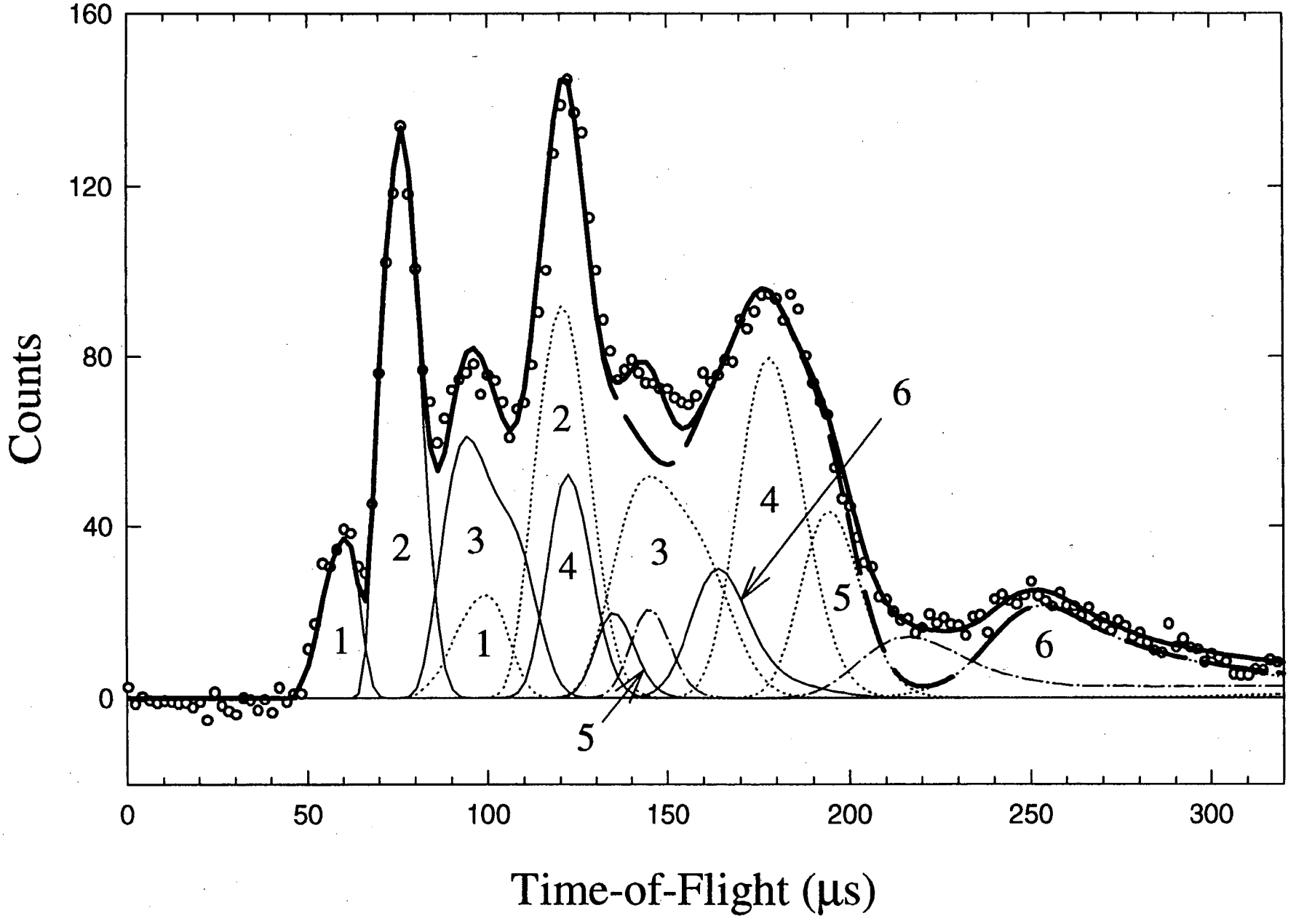
160
120
80
40
0
Counts
0
50
100
150
200
250
300
Time-of-Flight (μs)
1
2
3
4
5
6

Fig. 4

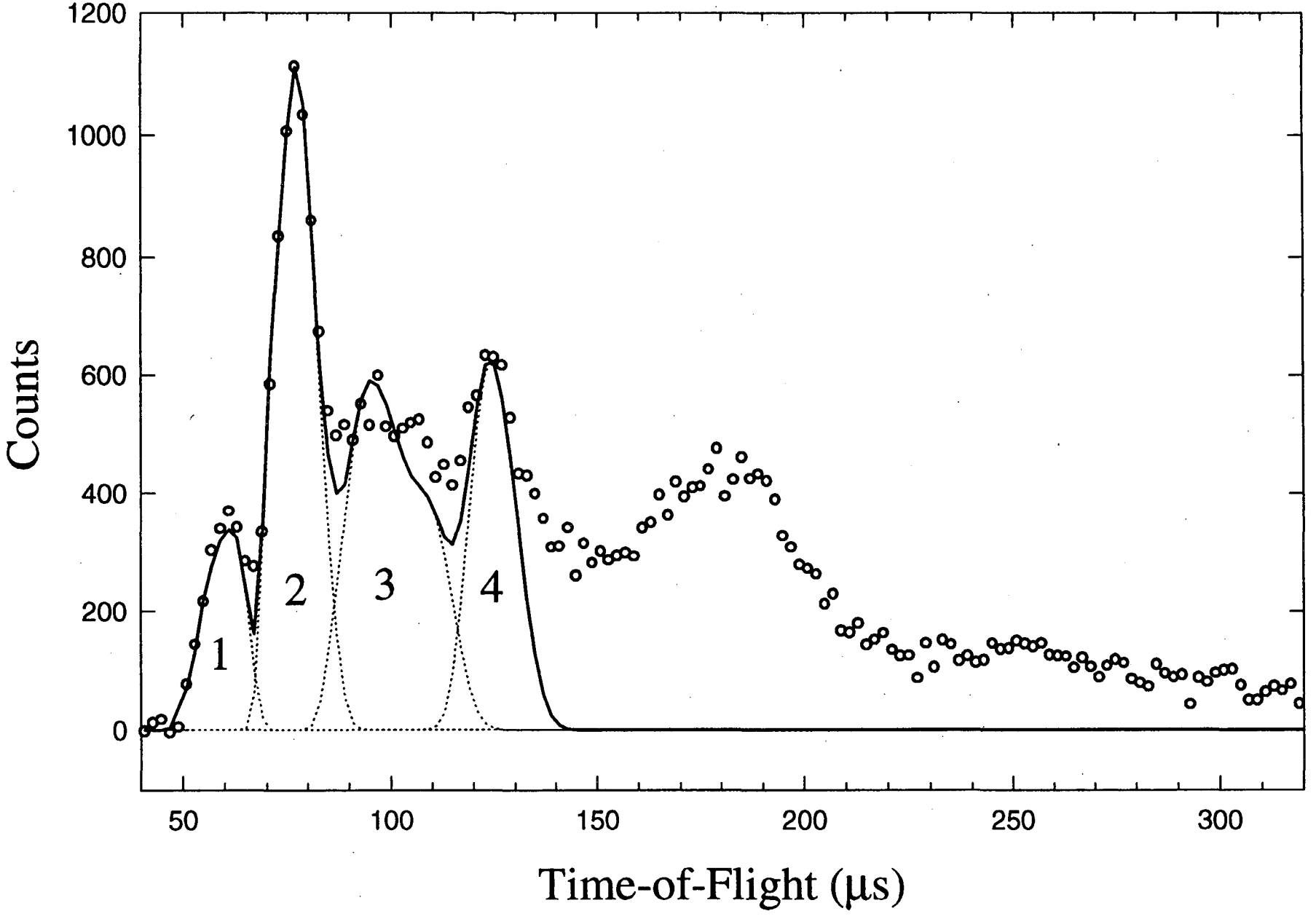
1200
1000
800
600
400
200
0
Counts
1
2
3
4
50
100
150
200
250
300
Time-of-Flight (μs)

Fig. 5

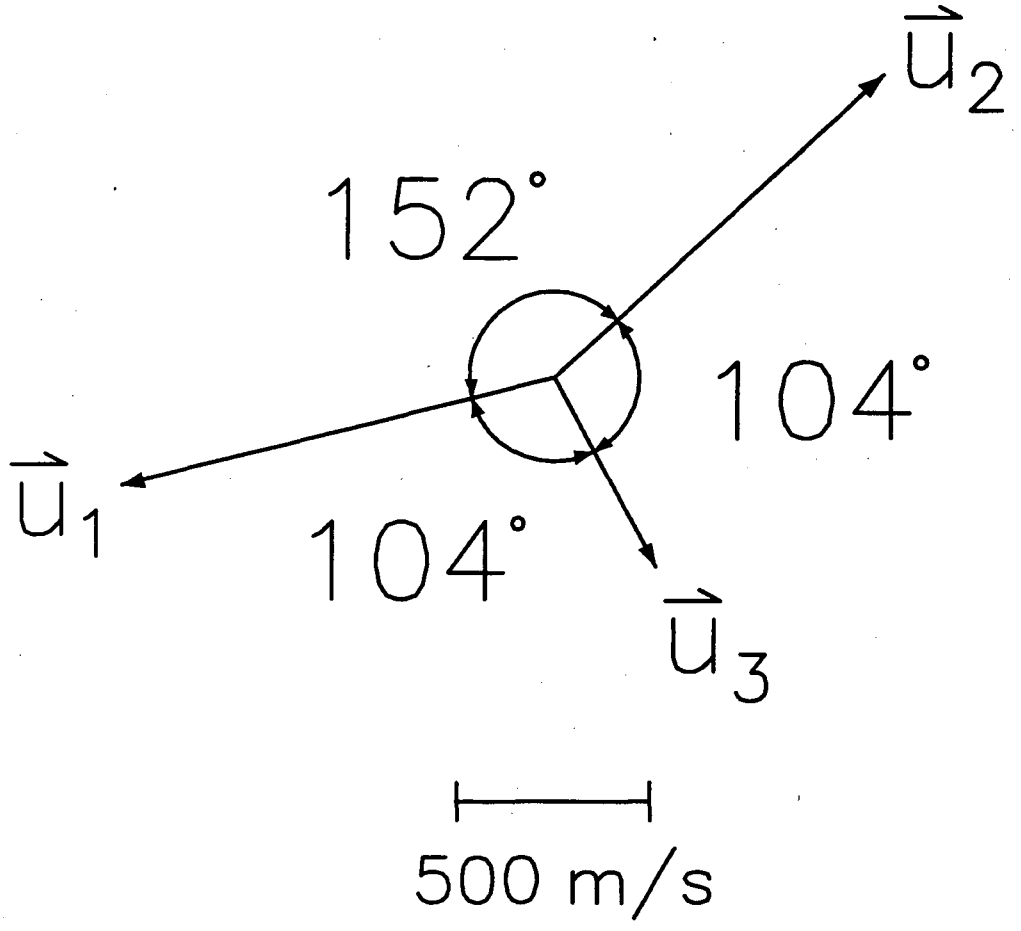

	$\vec{u}$ (m/s)	E_T (kcal/mol)
m_1	1155	2.55
m_2	1155	2.55
m_3	559	0.60

Fig. 6

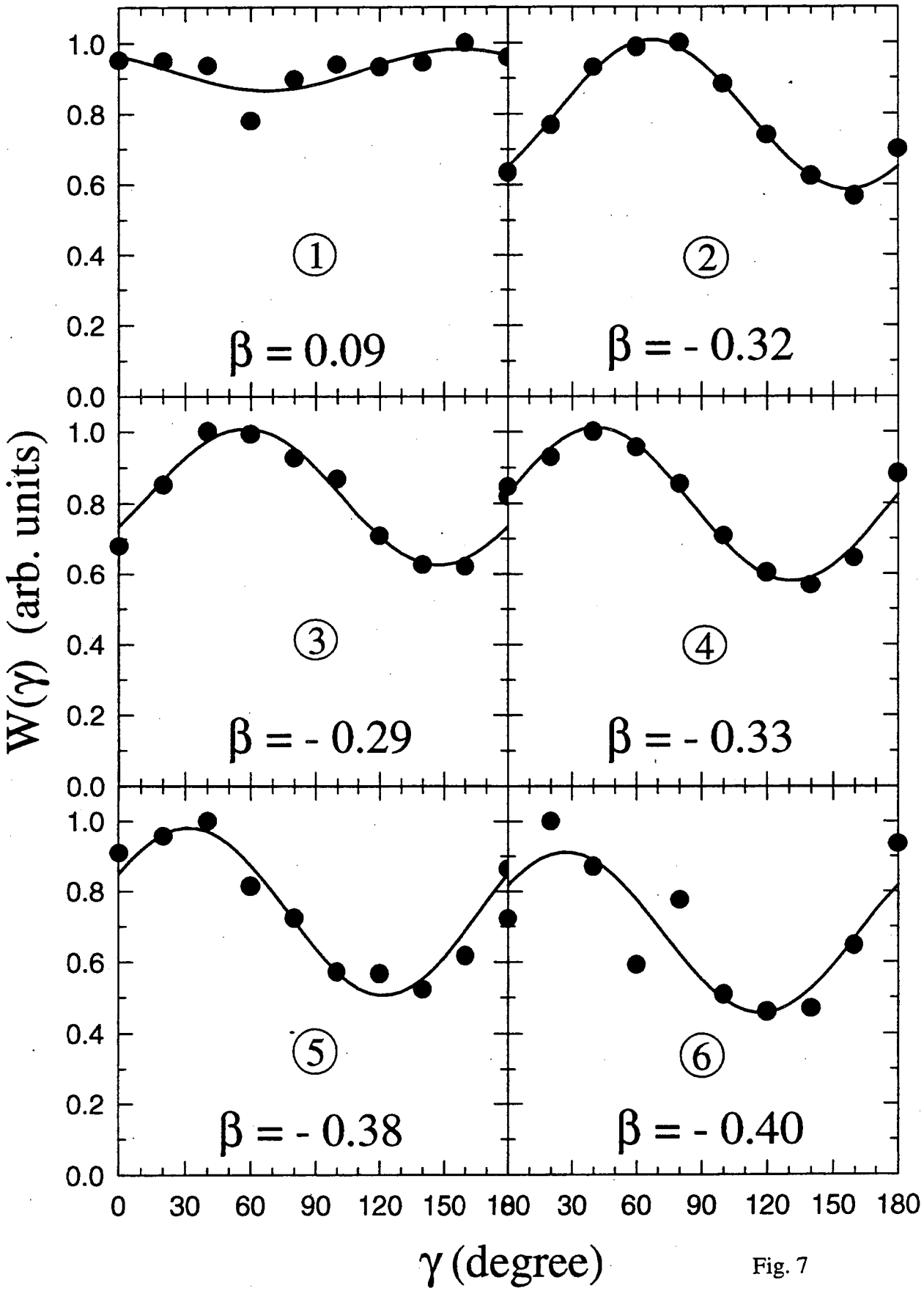
W(γ) (arb. units)
γ (degree)
1
β = 0.09
2
β = - 0.32
3
β = - 0.29
4
β = - 0.33
5
β = - 0.38
6
β = - 0.40
0.0
0.2
0.4
0.6
0.8
1.0
0
30
60
90
120
150
180

Fig. 7

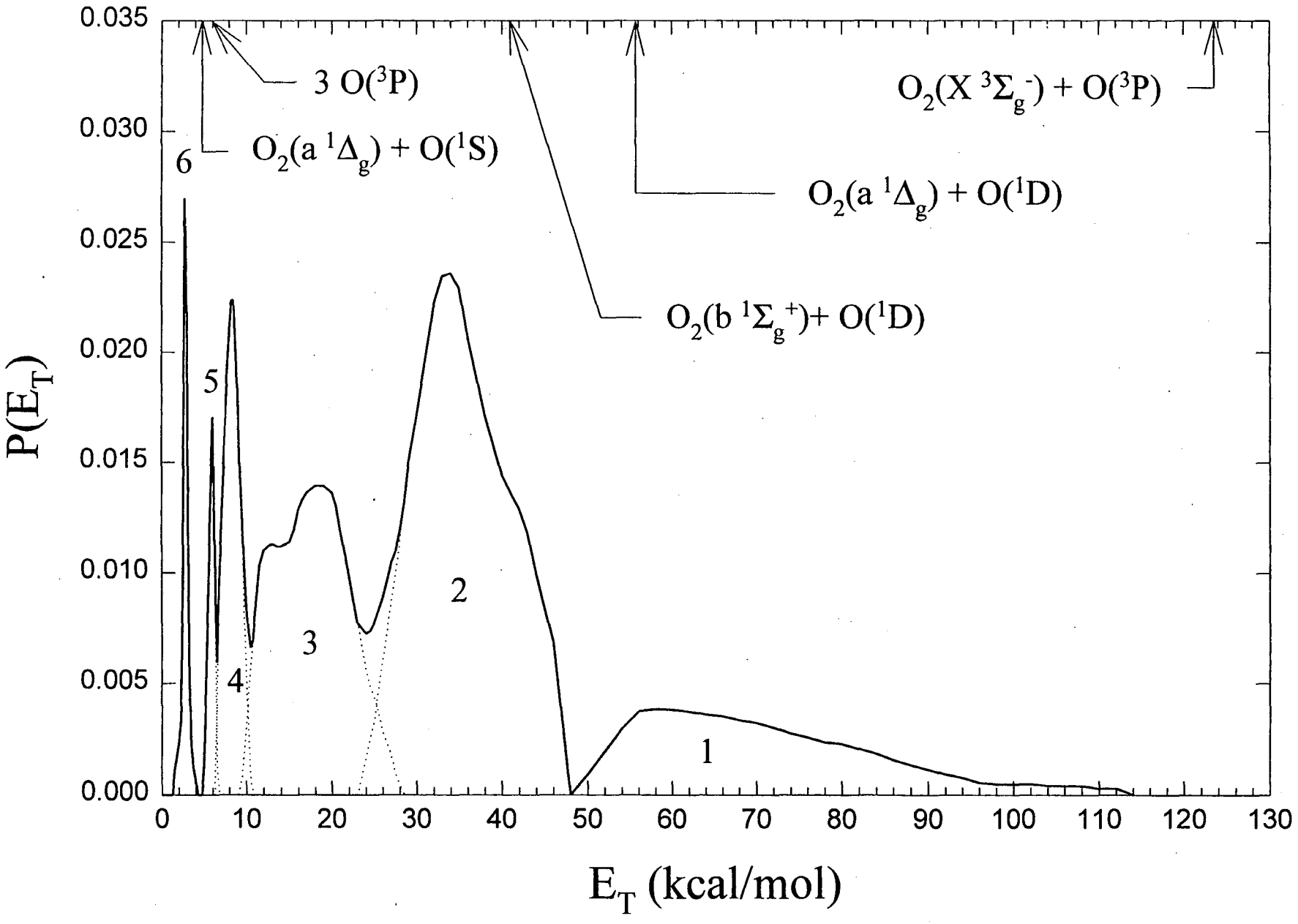
0.035
0.030
0.025
0.020
0.015
0.010
0.005
0.000
P(E_T)
0
10
20
30
40
50
60
70
80
90
100
110
120
130
E_T (kcal/mol)
3 O(3P)
O2(a 1Δg) + O(1S)
O2(X 3Σg-) + O(3P)
O2(a 1Δg) + O(1D)
O2(b 1Σg+)+ O(1D)
6
5
4
3
2
1

Fig. 8

LAWRENCE BERKELEY LABORATORY
UNIVERSITY OF CALIFORNIA
TECHNICAL INFORMATION DEPARTMENT
BERKELEY, CALIFORNIA 94720